Chemical Vapor Deposition of Mesoporous Graphene Nano-Balls for Supercapacitor.

4 AUTHORS, INCLUDING:

Jung-Soo Lee
Chosun University

21 PUBLICATIONS **342** CITATIONS
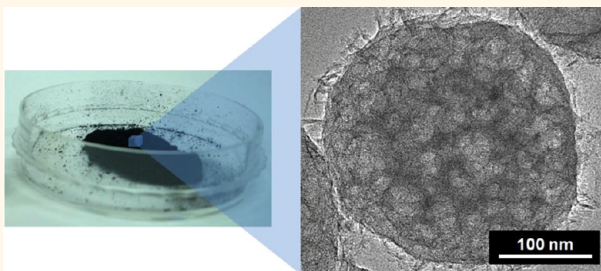
Chemical Vapor Deposition of Mesoporous Graphene Nanoballs for Supercapacitor

Jung-Soo Lee,[†] Sun-I Kim,[†] Jong-Chul Yoon, and Ji-Hyun Jang*

Interdisciplinary School of Green Energy, Low Dimensional Carbon Materials Center and KIER-UNIST Advanced Center for Energy, 689-798 UNIST, Ulsan, Korea. [†]These authors contributed equally to this work.

ABSTRACT A mass-producible mesoporous graphene nanoball (MGB) was fabricated *via* a precursor-assisted chemical vapor deposition (CVD) technique for supercapacitor application. Polystyrene balls and reduced iron created under high temperature and a hydrogen gas environment provide a solid carbon source and a catalyst for graphene growth during the precursor-assisted CVD process, respectively. Carboxylic acid and sulfonic acid functionalization of the polystyrene ball facilitates homogeneous dispersion of the hydrophobic polymer template in the metal precursor solution, thus, resulting in a MGB with a uniform number of graphene layers. The MGB is shown to have a specific surface area of 508 m^2/g and is mesoporous with a mean mesopore diameter of 4.27 nm. Mesopores are generated by the removal of agglomerated iron domains, permeating down through the soft polystyrene spheres and providing the surface for subsequent graphene growth during the heating process in a hydrogen environment. This technique requires only drop-casting of the precursor/polystyrene solution, allowing for mass-production of multilayer MGBs. The supercapacitor fabricated by the use of the MGB as an electrode demonstrates a specific capacitance of 206 F/g and more than 96% retention of capacitance after 10,000 cycles. The outstanding characteristics of the MGB as an electrode for supercapacitors verify the strong potential for use in energy-related areas.

KEYWORDS: graphene · mesoporosity · supercapcitor · chemical vapor deposition

Supercapacitors have attracted increasing attention due to their long life cycle, highly reversible charge storage process, and high specific power density along with increased concern over the exhaustion of natural resources.[1−4] Among the commonly used active materials such as conducting polymers and metal oxides, carbon materials such as carbon aerogels, porous carbons, and carbon nanotubes (CNTs) have been intensively studied due to their low price, fairly inert electrochemistry, reasonable electrical conductivity, and high specific surface area.[5−9] In particular, porous carbon materials have been suggested as effective electrodes for supercapacitors due to their large surface area and size tunable porosity for easy access of the electrolyte.[10−14] More specifically, effective surface area and pore volume in the nanostructure provide active sites for better performance of the supercapacitor, which operates *via* a mechanism of charge-separation at the electrochemical interface between the electrode and electrolyte.

In the past few years, graphene, a single layer carbon sheet with sp^2-hybridized hexagonal lattices, has been recognized as a promising active material of supercapacitors due to its superior electrical conductivity and high surface area, as these are the two most important requirements for supercapacitors.[15−18] From this point of view, among the various methods available for the fabrication of graphene sheets, chemical vapor deposition (CVD) growth on a metal substrate (Ni, Cu, *etc.*) is highly recommended, because the condutivities of graphene grown by CVD are much better than those of chemically synthesized graphene.[19−21]

Recent studies on the application of graphene-based elctrodes for supercapacitors have focused on achieving large surface area approaching the theoretical surface area *via* nanostructuring.[22−28] For instance, Ruoff *et al.* reported a great increase in the

surface area of graphene by the activation of a graphene oxide with KOH.[29] Cheng et al. attained increased surface area of active materials by the direct growth of graphene on a macro-sized metal-frame (Ni foam).[30] However, the former might have relatively low electrical conductivity as chemically fabricated graphene is used as a precursor and the latter has only macro-pores of a few hundred micrometers in diameter due to the restricted dimensions of the available metal template. Therefore it is crucial to ensure both good conductivity and large effective surface area of an electrode material for optimal performance of supercapacitors.

Herein, we report a unique route to obtain a mass-producible mesoporous graphene nanoball (MGB) with large surface area and great conductivity via precursor-assisted CVD using metal precursors as a catalyst. The metal precursor solution uniformly coated onto −COOH and −SO$_3$H funtionalized polystyrene beads offers three-dimensional (3D) metal frames and assists the graphene growth via reduction of metal precursors into a metal catalyst during the CVD process. The massively produced few layer MGB presents a specific surface area of 508 m^2/g and a single-modal mesoporosity with a mean pore diameter of 4.27 nm. The conductivity of p-doped MGB was measured to be 6.5 S/cm. The MGB-based supercapacitor demonstrates an outstanding capacitance of 206 F/g and 96% retention of capacitance after 10,000 cycles even at a high current density of 20 A/g. The excellent performance of the MGB as an electrode for supercapacitors highlights its potential for use in energy related areas.

RESULTS AND DISCUSSION

The fabrication process of MGB starts by the functionalization of PS in order to obtain a uniform coating of the hydrophilic iron precursor solution onto the hydrophobic PS spheres, as illustrated in Figure 1a. Briefly, the synthesis of functionalized PS entails the following 2 steps: synthesis of carboxylated PS (PS-COOH: poly(styrene-co-methacrylic acid)) via emulsion polymerization and sulfonization of carboxylated PS (SPS-COOH: sulfonated poly(styrene-co-methacrylic acid)), as shown in Figure 1a (the detailed process is illustrated in Figure S1). PS-COOH spheres were synthesized first in order to enhance the dispersibility of the PS spheres in the aqueuous iron precursor solution where the subsequent sulfonation occurs. Because of the relatively low wettability of PS in aqueous solution, the aggregated COOH domains result in morphologically bumpy spheres (Figure S2a). However, the domains of COOH eventually mediate the wettability
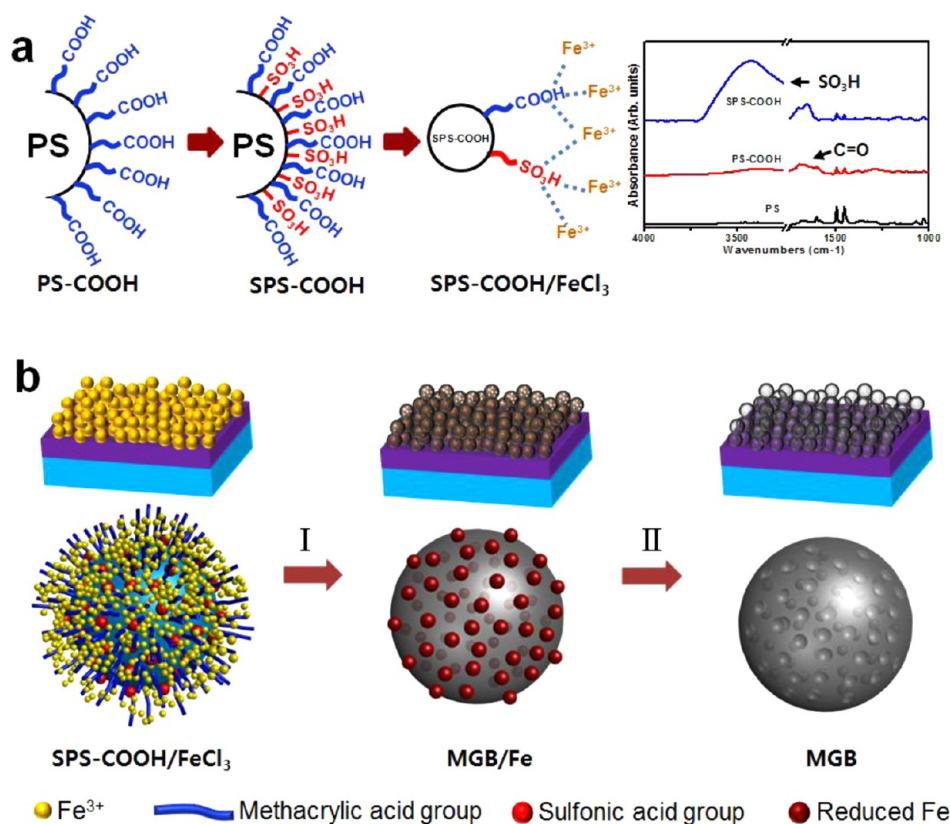

Figure 1. Schematic illustration of the mesoporous graphene nanoball (MGB). (a) The fabrication process of SPS-COOH (functionalization of PS via carboxylation and sulfonation) and the FT-IR spectra of the samples. (b) The fabrication process of MGB: step 1, drop casting of the SPS-COOH/FeCl$_3$ solution onto the substrate and subsequent CVD growth of graphene; step 2, the removal of iron domains to leave the MGB.

difference between the initial hydrophobic PS spheres and the aqueous solution, facilitating the formation of highly dispersible SPS-COOH spheres with a very smooth surface in the $FeCl_3$ solution, as shown in Figure S2b. FT-IR spectral changes of PS, PS-COOH spheres, and SPS-COOH spheres are shown in the right panel of Figure 1a and in Figure S3 (close-up image). The peak at 1697 cm^{-1} in both SPS-COOH and PS-COOH confirms the presence of a carbonyl group. The synthesis of SPS-COOH was verified by several distinct peaks related with the sulfonic group at 1125–1223 cm^{-1} and at around 3500 cm^{-1}.[31−33] The ratio of −COOH functional groups to −SO_3H functional groups was 1:0.68, measured by titration[34] and supported by zeta potential results (Figure S5). A homogeneous dispersion of SPS-COOH in the solution of the iron precursor derives from the electrostatic interaction between the strongly negatively charged groups (−COOH, −SO_3H) of SPS-COOH and iron ions (Fe^{3+}) in $FeCl_3$ solution, leading to adsorption of a sufficient amount of iron ions onto the spheres.[35] In fact, PS-COOH beads that are functionalized by a single COOH group did not create a uniform coating of $FeCl_3$, thus resulting in imperfect formation of the graphene layer. This is ascribed to the lower ionic strength of COOH as compared to that of SO_3H. We experimentally observed that a SO_3H/COOH ratio greater than 0.6 can lead to the formation of a homogeneous dispersion, therefore leading to uniform coverage of $FeCl_3$ and dense packing of aggregated Fe metals. For the fabrication of the MGB, the mixture of as-prepared SPS-COOH and $FeCl_3$ solution was drop-casted onto a 300 nm SiO_2/Si wafer and dried in a vacuum oven at room temperature, as shown in Figure 1b. We used iron chloride ($FeCl_3$) and highly dispersible SPS-COOH as a precursor of the iron catalyst and a solid carbon template for graphene growth, respectively. Iron has been intensively studied as a catalyst for carbon nanotube synthesis, and could also be utilized for the synthesis of graphene given the extensive information on its binary phase diagram with carbon.[36] Compared to common metal catalysts such as Cu and Ni, iron offers affordability, a mild etching process, and more importantly, a higher melting point, which helps to sustain the nanoscale morphology under the high temperature CVD conditions. The completely dried 3D composites of $FeCl_3$/SPS-COOH on the SiO_2/Si substrate were subsequently heated to 1000 °C in a quartz tube under a H_2/Ar atmosphere (I). During the process of annealing at high temperature (>700 °C) in the hydrogen atmosphere, SPS-COOH polymer spheres and iron ions undergo different transformations. About 95% of SPS-COOH was evaporated, as confirmed by the TGA curve (Figure S4), whereas the iron ions that had absorbed on the SPS-COOH surface *via* electro-static interaction were reduced into iron metal. Here, the reduced irons served as three-dimensional nanoframes (domains) as well as a catalyst

for growth of multilayer graphene. Nanodomains of iron clusters are created from the agglomeration of iron particles followed by the percolation of iron into the soft PS spheres at high temperature annealing conditions. The ratio of $FeCl_3$ to SPS-COOH was carefully controlled to determine both the minimum amount of residual amorphous carbon and appropriate content of iron, as shown in Figure S6. Finally, a reduced iron framework was etched away in a 3% HCl solution for 6 h, leaving a MGB structure (II, step 2).

To utilize Fe(0) as a metal catalyst for initiation of the graphene growth, it is critical to fully convert Fe(III) to Fe(0). To confirm that Fe(III) is reduced into Fe(0), we performed X-ray diffraction measurements. Figure 2a shows the XRD pattern of the SPS-COOH/$FeCl_3$ mixture before and after annealing in a H_2/Ar atmosphere. In contrast with the data taken from the pristine SPS-COOH/$FeCl_3$ film where there was no significant peak except a gently raised SiO_2/Si substrate peak at $2\theta = 70°$ (in black), one strong peak corresponding to the (110) plane of Fe (JCPDS 01-071-3763) and another peak at $2\theta = 26°$ corresponding to the (002) plane of graphitic carbon (JCPDS 01-075-1621) are evolved for the annealed sample (in red). Additionally, several peaks indexed to Fe_3C (JCPDS 98-000-0170) were also observed at the regions marked with inversed triangles. It is known that both Fe_3C and Fe can act as catalysts for the growth of carbon nanotubes and nanofibers[37−39] which could be applicable to the graphene growth. The results imply that reduced iron in the mesoporous iron/carbon is polycrystalline, consequently resulting in the formation of multilayer graphene. The solid carbon source provided by PS spheres results in some residual carbon even after the segregation process, leading to amorphous characteristics of MGB with defect regions and thus rather weak intensity of the carbon peak in the XRD pattern. The left image in Figure 2b shows the readily dispersible SPS-COOH in $FeCl_3$ solutions after functionalization of PS and the right image displays the mass-producible multilayer graphene obtained by the CVD of the sample. As can be seen in the digital camera image in Figure 2b, we obtained gram scale multilayer graphene nanoballs after the precursor-assisted CVD process of dried $FeCl_3$/SPS-COOH. X-ray photoelectron spectroscopy (XPS) further confirmed the transformation of SPS-COOH/$FeCl_3$ under the CVD conditions. Figure 2c, d shows XPS spectra of Fe and C of the sample before and after the CVD.[39] The transition of Fe (3^+) into Fe(0) is verified by the appearance of the peak at 706.68 eV (in red, after CVD growth) and the disappearance of the peak at 711.48 eV (in black, before CVD growth) that corresponds to Fe 2p. The black curve in XPS spectrum of C is deconvoluted into red, blue, pink, and green curves representing the specfic binding states of each functional group, as shown in Figure 2d. Compared to the XPS peak of C
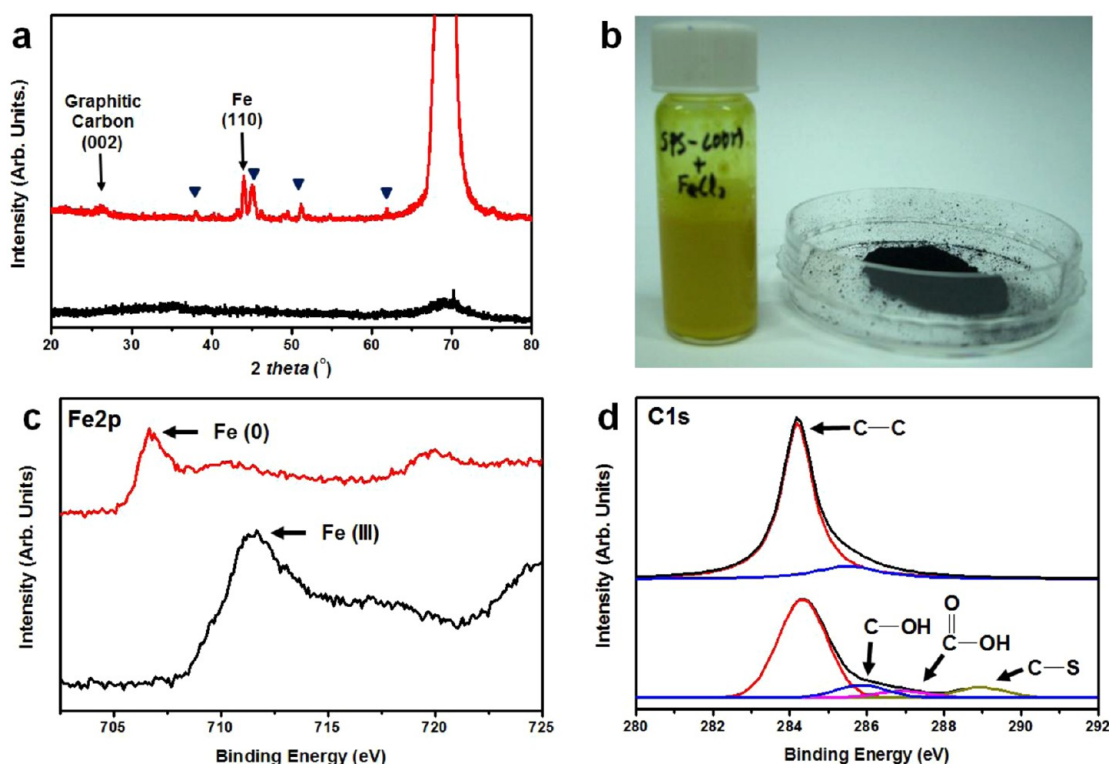
Figure 2. Characterization of of SPS-COOH/FeCl$_3$ before (in black) and after (in red) CVD. (a) XRD patterns; (b) photographic images of the sample before (left) and after (right) the CVD processes; (c and d) XPS spectra of Fe and C of the sample. The black curve was decomposed into superposed red, blue, and pink curves representing the specific binding states of each functional group in panels d. All upper images represent the samples after the CVD, whereas the lower images represent those before the CVD procedure in panels a, c, and d.

that is decomposed into several peaks from many oxygen containing extra bonds in FeCl$_3$/SPS-COOH (bottom, before CVD growth), the XPS analysis of MGB (top) with an intense C=C/C—C bond peak at 284.18 eV and only a small peak originating from the C—O bonds ensures reasonable quality of the MGB.[40,41]

Figure 3 shows the morphological observation of the polymeric spheres and MGB created by precursor-assisted CVD growth. The scanning electron microscope (SEM) image in Figure 3a reveals that SPS-COOH spheres with a diameter of around 250 nm are nearly uniform in size and morphology. It is very important to obtain an appropriate dispersion in FeCl$_3$ solution for obtaining uniform size and shape of MGB. As can be seen from the smooth surface morphology, the styrene part in the surface of PS-COOH was rendered much hydrophilic by sulfonation of PS-COOH, via an electrophilic substitution reaction at the para-position of styrene, creating a highly dispersed SPS-COOH aqueous solution (Figure S1). Note that the use of single type of PS-COOH beads causes imperfect formation of the graphene layer due to insufficient coating of FeCl$_3$, thus, resulting in the collapse of the nanoball after the removal of iron domains. A comparison of the features of PS-COOH and SPS-COOH (Figure S2) verifies that our two-step preparation method via functionalization of PS has successfully overcome the problem of agglomeration of COOH groups on the surface of PS in the aqueous

solution. Figure 3b is a SEM image of MGB fabricated from FeCl$_3$/SPS-COOH. Polymeric spheres were successfully converted to MGB via precursor-assisted CVD in a H$_2$/Ar atmosphere without any remarkable collapse of the spherical shape. Close inspection by high resolution TEM verifies the formation of a mesoporous graphene nanoball with a mean pore diameter of 4.27 nm, as shown in Figure 3c,d. These mesopores are created from the removal of the iron domains, formed due to the aggregation and subsequent percolation of iron into the soft SPS-COOH spheres at the high temperature annealing conditions. The inset of Figure 3c confirms the formation of multilayer graphene with a lattice spacing of 3.4 A.

Figure 4a shows the Raman data of FeCl$_3$/SPS-COOH (in black) with an optimized ratio and corresponding MGB (in red) fabricated via the precursor-assisted CVD method. The presence of broad D and G bands at around 1350 and 1580 cm^{-1}, in combination with the absence of 2D band at 2700 cm^{-1} for the pristine polymer sphere, reveals the amorphous characteristics of FeCl$_3$/SPS-COOH. In contrast, the sharp G and 2D bands and reduced D band in MGB (red) clearly demonstrate the creation of few-layer graphene. The maximum ratio of I_{2D}/I_g of 0.87 and the minimum ratio of I_d/I_g of 0.46 with the full width at half-maximum (fwhm) of 44.6 indicate a reasonable quality MGB (fwhm of single layer graphene ≈33).
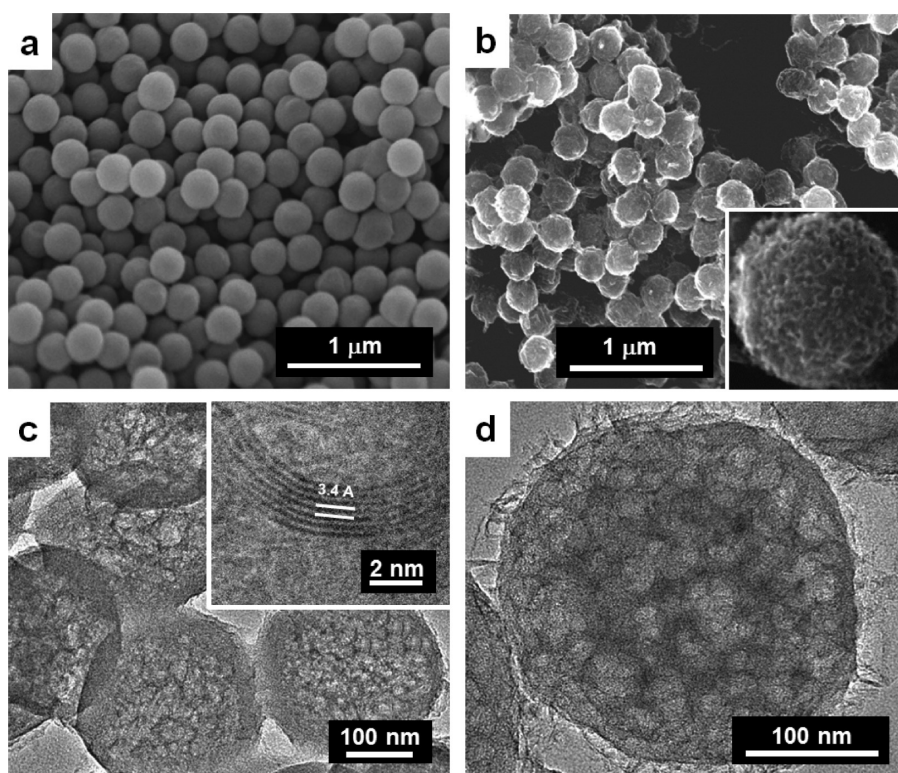
Figure 3. SEM images of (a) SPS-COOH and (b) MGB obtained by CVD of sample (a). The inset in panel b shows the close-up SEM image of mesoporous single graphene ball. (c) TEM images of MGB taken near the edges of the sample. The inset confirms ~7 layers of MGB with an interlayer spacing of 0.34 nm. (d) Magnification image of a single graphene ball with mesopores.
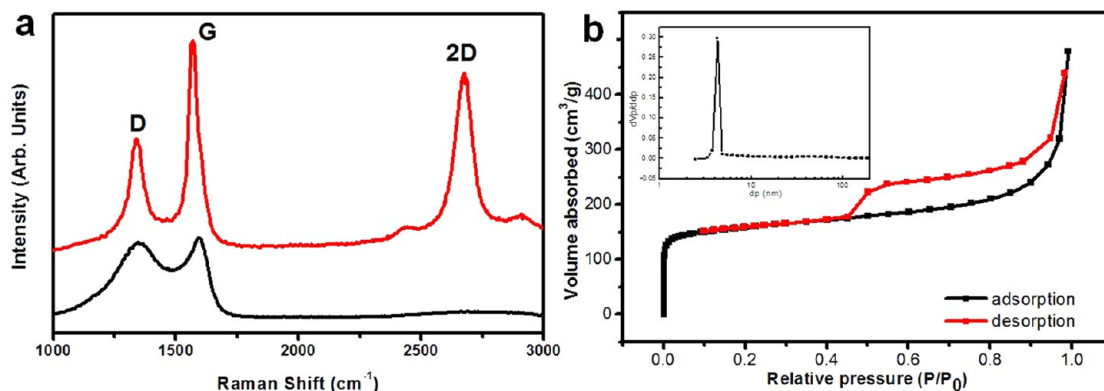

Figure 4. (a) Raman spectra of SPS-COOH/FeCl$_3$ before (lower) and after (upper, MGB) CVD growth of graphene. (b) The N$_2$ adsorption−desorption isotherm loop of MGB. The inset is a histogram of the pore size distribution (PSD).

The specific surface areas and the pore size distribution plots of MGB were obtained using the Brunauer−Emmett−Teller (BET) method *via* N$_2$ adsorption isotherms and the Barrett−Joyner−Halenda (BJH) method. The shape of the isotherm in Figure 4b is classfied as type IV, indicating the presence of mesopores in the structure. The surface area and pore volume of MGB were 508 m^2/g and 0.74 cm^3/g, respectively. The BJH pore size distribution reveals a mesoporosity of MGB with an average pore size of 4.27 nm, calculated through the desorption isotherm, as shown in the inset of Figure 4b. Such high surface area is uncommon for

simple PS spheres (the surface area of same size PS spheres is 15.1 m^2/g) and is due to the presence of a large fraction of mesopores in the graphene ball.

To evaluate the properties of MGB as an electrode material for supercapacitors, we performed electrochemical measurements in a voltage range from −0.5 to 0.3 V. Here, MGB was p-doped by dipping in H$_2$SO$_4$ to further enhance the conductivity, which has a crucial impact on the capacitance value of a supercapacitor. It has been reported that the electronic properties of graphene can be modified by doping the sulfur onto the graphene plain due to the structural
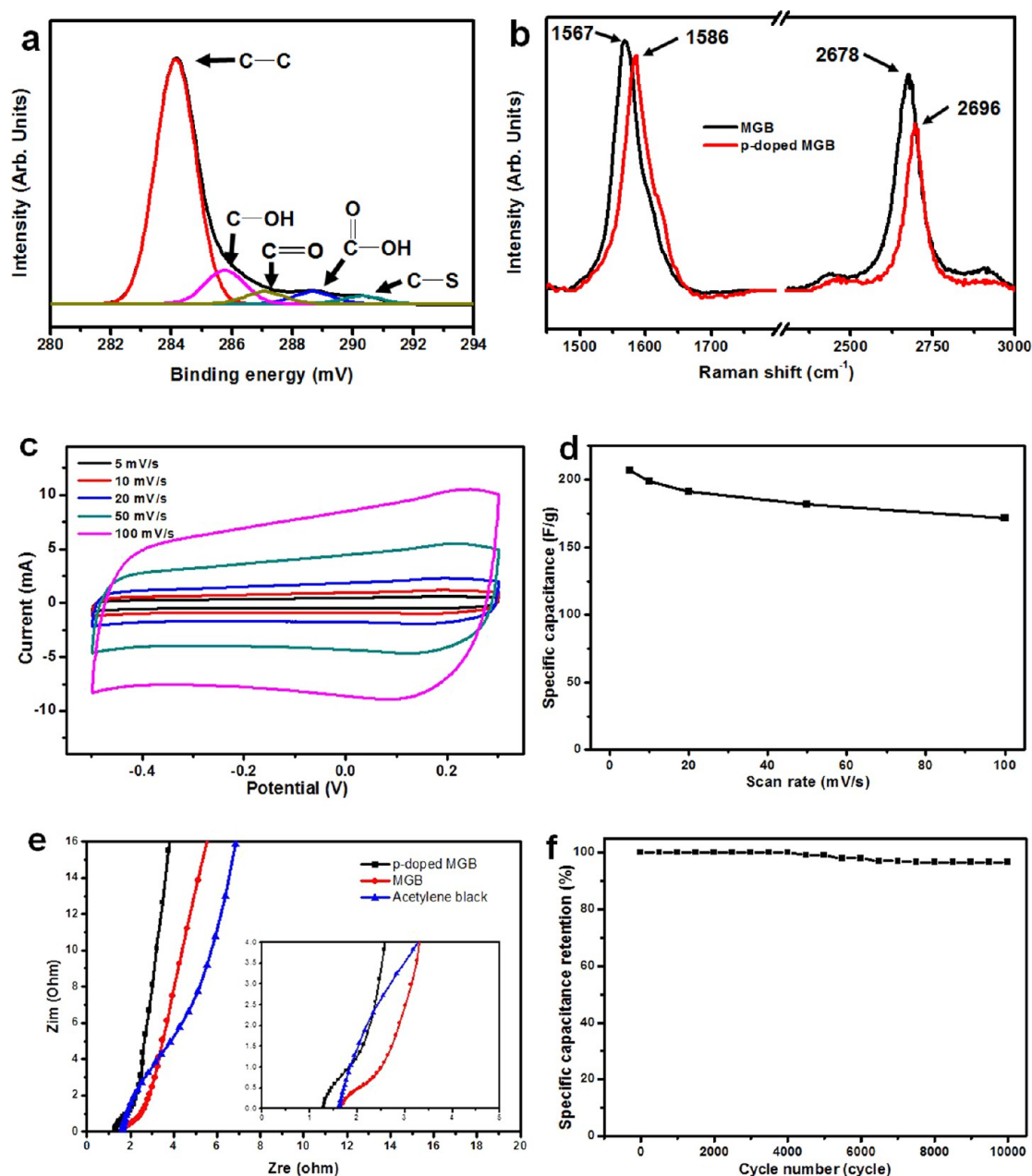
Figure 5. (a) C1s XPS spectra and (b) Raman spectra of MGB and p-doped MGB. (c) Cyclic voltammetry curves of p-doped MGB in a voltage range from −0.5 to 0.3 V and (d) specific capacitance with increasing scan rate. (e) Nyquist plots of MGB, p-doped MGB, and acetylene black as a reference material. The inset is the close-up EIS image in the high frequency region. (f) Cycle performance of p-doped MGB-based supercapacitor at a current density of 20 A/g.

changes induced by the sulfuric acid and oxide groups, which affect the π electrons of carbon atoms. Figure 5a shows the C1s XPS spectrum of p-doped MGB with a strong peak at 284.18 eV, originating from C−C and C=C and a raised shoulder peak that is deconvoluted into several peaks at 285.5, 287.4, and 289.3 eV, corresponding to C=O, C−(OH), and C−S. The spectrum confirms the incorporation of sulfuric acid and oxide groups during the doping process (XPS data of O1s and S2p are shown in Figure S10). Both the G peak and 2D peak in Raman spectra are shifted to lower energy, due to the additional defects in the graphene

lattice, caused by incorporating heteroatoms, which is in accordance with a previous report on p-doped graphene.[42] The large peak shift indicates that MGB is strongly p-doped and, as a result, the conductivity of MGB was raised from 1.7 to 6.5 S/cm after doping, as shown in Figure S11. However, unexpectedly, the BET and BJH results of p-doped MGB reveal a reduction of surface area from 508 to 346 m^2/g while retaining a mean mesopore diameter of 4.27 nm after doping (Figure S12). This may be attributed to the incorporation of heavy sulfur and oxygen atoms onto the graphene lattice during the doping process, inducing

an increase in the density of the samples, and thus a decrease in the specific surface area. Figure 5c shows the CV curves of the p-doped MGB electrode at different scan rates. The relatively rectangular shape of the CV even at a high voltage scan rate confirms traditional double-layer capacitance characteristics with a negligible contribution of the pseudocapacitance property from the faradic processes, which can occur at the oxygen groups in the p-doped MGB. The specific capacitance slightly decreased from 206 F/g to 191 F/g with an initial increase of the voltage scan rate from 5 to 20 mV/s and then remained almost unchanged for a scan rate range of 20 to 100 mV/s. The outstanding specific capacitance of p-doped MGB with relatively low surface area (346 m^2/g) is attributed to the excellent electrical conductivity of pristine MGB achieved *via* a CVD-graphene growth process, which is supported by previous reports.[43,44] The enhanced conductivity of p-doped MGB can be further explained by the EIS data, which show characteristics of various electrochemical processes at specific operating frequency ranges in the equivalent circuit. EIS measurements of the p-doped MGB, MGB, and acetylene black as a control sample were carried out to evaluate the intrinsic resistance, as shown in Figure 5e. The partial semicircles in the high frequency region (in the inset) reflect the characteristic of the process occurring at the carbon electrode—electrolyte interface due to the conductivity difference between the carbon electrode (electronic conductivity) and liquid electrolyte path (ionic conductivity). The obvious difference in the diameter of the semicircles indicates that both the MGB and p-doped MGB with greater conductivity have much lower resistance in charge propagation at the interface between the electrode/electrolyte than the acetylene black. The impedance behavior of MGBs at the medium frequency region is characteristic of a surface reaction induced by charge-transfer resistance, as shown in Figure 5e. Compared to the relatively slanted lines of MGB and acetylene black reference sample, the vertical-line feature of p-doped MGB close to 90° indicates good capacitive behavior and low diffusion resistance of ions

in the structure of the electrode due to the mesoporous surface morphology, which provides better accessibility to the electrolyte even at a higher current density condition. Moreover, by doping MGB with sulfuric acid groups, the surface wettability is improved, resulting in a beneficial impact on accessibility of electrolytes. Therefore, the great specific capacitance of p-doped MGBs is attributed to the large accessible and effective surface area achieved by proper-sized mesopores of 4.27 nm, offering advantages in transport of the electrolyte as well as high electronic conductivity of p-doped MGBs. (Charge/discharge curves at different current densities are shown in Figure S13.) Further, the MGB sample was tested for potentiostatic charge—discharge cycles at a current density of 20 A/g to evaluate its long-term stability. The capacitance retention of the MGB sample after 10,000 charge/discharge cycles is found to be a reasonable value of 96% even at a high current density, as shown in Figure 5f. This demonstrates that repeated charge/discharge does not appear to cause a significant structural change to the MGB electrode.

CONCLUSION

We have developed a direct method for mass-producible fabrication of mesoporous graphene nanoballs from a polymer/metal precursor solution *via* a precursor-assisted CVD process. The MGB presents a specific surface area of 508 m^2/g and mesoporosity with mean pore diameters of 4.27 nm. The mesopores were created from the aggregation and subsequent percolation of iron into the soft SPS-COOH spheres at high temperature annealing conditions, followed by the removal of the iron domains. The conductivity of the p-doped MGB obtained from more than 10 samples was 6.5 S/cm. The MGB-based supercapacitor shows good performance, including an excellent capacitance of 206 F/g and 96% retention of capacitance after 10,000 cycles even at a high current density. The outstanding perfomance of MGB as an electrode for supercapacitors highlights its potential for use in a variety of applicaitons.

METHOD

Synthesis of Sulfonated Poly(styrene-*co*-methacrylic acid) (SPS-COOH) Sphere. Poly(styrene-*co*-methacrylic acid) spheres were prepared by an emulsion polymerization method. The preparation of poly(styrene-*co*-methacrylic acid) spheres was accomplished as follows. Styrene (10 mL), methacrylic acid (1 mL), and deionized (D.I.) water (100 mL) were introduced into a 250 mL two-necked flask equipped with a magnetic stirring device, a reflux condenser, a nitrogen inlet, and a temperature controller. After purging the reaction mixture *via* N$_2$ bubbling for 30 min, the temperature was increased to 70 °C and then 2 mL of potassium persulfate (0.25 g/10 mL water) was added as a initiator to start the polymerization process. The reaction was allowed to proceed for 2.5 h and poly(styrene-*co*-methacrylic acid) spheres were obtained as a stable dispersion in water.

For the synthesis of sulfonated poly(styrene-*co*-methacrylic acid) spheres, 100 mL of concentrated sulfuric acid was added dropwise into a poly(styrene-*co*-methacrylic acid) sphere dispersion mixture in an ice bath and then held at 40 °C for 8 h.[45] The prepared sulfonated poly(styrene-*co*-methacrylic acid) spheres were filtrated and washed several times with D.I. water and ethanol, respectively.

Synthesis of Mesoporous Graphene Nanoballs (MGBs). SPS-COOH (1 g) was fully dispersed in D.I. water (16 g) and then FeCl$_3$ (4 g) was added in an ice bath. The dried SPS-COOH/FeCl$_3$ mixture was placed in a quartz tube (Scientech Co.) with an outer diameter of 2 in., heated to 1000 °C under a H$_2$ (100 sccm)/Ar (200 sccm) atmosphere with a heating rate of ∼100 °C/min, and then placed in isothermal conditions for 30 min. After annealing, the samples were rapidly cooled to ambient temperature.

Reduced iron in the sample was etched away in HCl 3% for 6 h to obtain a pure MGB. MGB was p-doped by dipping in 1 M H_2SO_4 solution for 3 h at 120 °C followed by washing in D.I. water in order to enhance the conductivity for supercapacitance measurements.

Characterization. The structures of the samples were characterized by SEM (Nova Nano-SEM 230, 15 kV), TEM (JEM-2100, 200 kV) and Raman spectroscopy (WITec, alpha300R, excited by a 532 nm laser). X-ray diffraction measurements were carried out with a Rigaku Co. High Power X-ray Diffractometer D/MAZX 2500 V/PC from 10° to 80°. The variation of the chemical structure was confirmed by FT-IR (Agilent; ATR mode). Surface area determination was performed by Brunauer—Emmett—Teller (BET) methods using an Belsorp-max (Bel Japan, Inc.) surface area analyzer. To measure conductivity of powder type MGB, the pellet with a diameter of 13 mm and thickness of 20 μm was prepared by mechanical milling and subsequent pressurizing (1000 kg/cm^2) of the MGB. The conductivity was obtained with the equation of $\sigma = 1/(R \times d)$, where d is the thickness of the sample and R is the sheet resistance of the sample. The sheet resistance of MGB was characterized by 4 point-probe (Dasol Eng, FPP-RS8, pin-spacing 1 mm, pin-radius 100 μm).

Electrochemical Measurement. The electrochemical properties of supercapacitor electrodes were measured in three-electrode systems by cyclic voltammetry using a computer controlled electrochemical interface (Solartron SI 1287) from −0.5 to 0.3 V at room temperature.[46,47] MGB, a graphite plate, Ag/AgCl, and 1 M H_2SO_4 were used as the working electrode, counter electrode, reference electrode, and electrolyte, respectively. To measure the electrochemical properties, the electro-active material (MGB) was mixed with acetylene black (10 wt %), and polyvinylidene floride (PVDF, 10 wt %) as a binder, and then the mixture was pasted onto a stainless steel electrode (1 cm X 1 cm) and dried at 150 °C for 20 min in an air atmosphere. The cyclic voltammetry was carried out at different scan rates ranging from 5 to 100 mV/s. Electrochemical impedance spectroscopy (EIS) was carried out at a frequency range from 100 kHz to 0.1 Hz using a potentiostat (Versa STAT 3, AMETEK). The control sample for EIS measurement was fabricated with 90 wt % of acetylene black and 10 wt % of PVDF.

Conflict of Interest: The authors declare no competing financial interest.

Supporting Information Available: Additional experimental details and further analysis results. This material is available free of charge *via* the Internet at http://pubs.acs.org.

REFERENCES AND NOTES

1. Conway, B. E. *Electrochemical Supercapacitor: Scientific Fundamentals and Technological Applications*; Pleum: New York, 1999.
2. Kötz, R.; Carlen, M. Principles and Applications of Electrochemical Capacitors. *Electrochim. Acta* **2000**, *45*, 2483–2498.
3. Wang, G.; Zhang, L.; Zhang, J. A Review of Electrode Materials for Electrochemical Supercapacitors. *Chem. Soc. Rev.* **2012**, *41*, 797–828.
4. Hao, Q. L.; Wang, H. L.; Yang, X. J.; Lu, L. D.; Wang, X. Morphology-Controlled Fabrication of Sulfonated Graphene/Polyaniline Nanocomposites by Liquid/Liquid Interfacial Polymerization and Investigation of Their Electrochemical Properties. *Nano Res.* **2011**, *4*, 323–333.
5. Chien, H.-C.; Cheng, W.-Y.; Wang, Y.-H.; Lu, S.-Y. Ultrahigh Specific Capacitances for Supercapacitors Achieved by Nickel Cobaltite/Carbon Aerogel Composites. *Adv. Funct. Mater.* **2012**, *22*, 5038–5043.
6. Frackowiak, E. Carbon Materials for Supercapacitor Application. *Phys. Chem. Chem. Phys.* **2007**, *9*, 1774–1785.
7. Zhang, L. L.; Zhao, X. S. Carbon-Based Materials as Supercapacitor Electrodes. *Chem. Soc. Rev.* **2009**, *38*, 2520–2531.
8. Choi, B. G.; Chang, S. J.; Kang, H. W.; Park, C. P.; Kim, H. J.; Hong, W. H.; Lee, S.; Huh, Y. S. High Performance of a Solid-State Flexible Asymmetric Supercapacitor Based on Graphene Films. *Nanoscale* **2012**, *4*, 4983–4988.
9. Jiang, H.; Li, C. Z.; Sun, T.; Ma, J. A Green and High Energy Density Asymmetric Supercapacitor Based on Ultrathin MnO_2 Nanostructures and Functional Mesoporous Carbon Nanotube Electrodes. *Nanoscale* **2012**, *4*, 807–812.
10. Ania, C. O.; Khomenko, V.; Raymundo-Piñero, E.; Parra, J. B.; Béguin, F. The Large Electrochemical Capacitance of Microporous Doped Carbon Obtained by Using a Zeolite Template. *Adv. Funct. Mater.* **2007**, *17*, 1828–1836.
11. Li, W.; Chen, D.; Li, Z.; Shi, Y.; Wan, Y.; Wang, G.; Jiang, Z.; Zhao, D. Nitrogen-Containing Carbon Spheres with Very Large Uniform Mesopores: The Superior Electrode Materials for EDLC in Organic Electrolyte. *Carbon* **2007**, *45*, 1757–1763.
12. Wang, D.-W.; Li, F.; Liu, M.; Lu, G. Q.; Cheng, H.-M. 3D Aperiodic Hierarchical Porous Graphitic Carbon Material for High-Rate Electrochemical Capacitive Energy Storage. *Angew. Chem., Int. Ed.* **2008**, *47*, 373–376.
13. Huang, C. H.; Zhang, Q.; Chou, T. C.; Chen, C. M.; Su, D. S.; Doong, R. A. Three-Dimensional Hierarchically Ordered Porous Carbons with Partially Graphitic Nanostructures for Electrochemical Capacitive Energy Storage. *ChemSusChem* **2012**, *5*, 563–571.
14. Lei, Z.; Christov, N.; Zhang, L. L.; Zhao, X. S. Mesoporous Carbon Nanospheres with an Excellent Electrocapacitive Performance. *J. Mater. Chem.* **2011**, *21*, 2274–2281.
15. Geim, A. K.; Novoselov, K. S. The Rise of Graphene. *Nat. Mater.* **2007**, *6*, 183–191.
16. Novoselov, K. S.; Geim, A. K.; Morozov, S. V.; Jiang, D.; Zhang, Y.; Dubonos, S. V.; Grigorieva, I. V.; Firsov, A. A. Electric Field Effect in Atomically Thin Carbon Films. *Science* **2004**, *306*, 666–669.
17. Zhang, L. L.; Zhao, X.; Stoller, M. D.; Zhu, Y.; Ji, H.; Murali, S.; Wu, Y.; Perales, S.; Clevenger, B.; Ruoff, R. S. Highly Conductive and Porous Activated Reduced Graphene Oxide Films for High-Power Supercapacitors. *Nano Lett.* **2012**, *12*, 1806–1812.
18. Xu, Y.; Lin, Z.; Huang, X.; Liu, Y.; Huang, Y.; Duan, X. Flexible Solid-State Supercapacitors Based on Three-Dimensional Graphene Hydrogel Films. *ACS Nano* **2013**, *7*, 4042–4049.
19. Reina, A.; Jia, X.; Ho, J.; Nezich, D.; Son, H.; Bulovic, V.; Dresselhaus, M. S.; Kong, J. Large Area, Few-Layer Graphene Films on Arbitrary Substrates by Chemical Vapor Deposition. *Nano Lett.* **2008**, *9*, 30–35.
20. Wu, W.; Jauregui, L. A.; Su, Z.; Liu, Z.; Bao, J.; Chen, Y. P.; Yu, Q. Growth of Single Crystal Graphene Arrays by Locally Controlling Nucleation on Polycrystalline Cu Using Chemical Vapor Deposition. *Adv. Mater.* **2011**, *23*, 4898–4903.
21. Chen, S.; Cai, W.; Piner, R. D.; Suk, J. W.; Wu, Y.; Ren, Y.; Kang, J.; Ruoff, R. S. Synthesis and Characterization of Large-Area Graphene and Graphite Films on Commercial Cu—Ni Alloy Foils. *Nano Lett.* **2011**, *11*, 3519–3525.
22. Wen, Z.; Wang, X.; Mao, S.; Bo, Z.; Kim, H.; Cui, S.; Lu, G.; Feng, X.; Chen, J. Crumpled Nitrogen-Doped Graphene Nanosheets with Ultrahigh Pore Volume for High-Performance Supercapacitor. *Adv. Mater.* **2012**, *24*, 5610–5616.
23. Ji, H.; Zhang, L.; Pettes, M. T.; Li, H.; Chen, S.; Shi, L.; Piner, R.; Ruoff, R. S. Ultrathin Graphite Foam: A Three-Dimensional Conductive Network for Battery Electrodes. *Nano Lett.* **2012**, *12*, 2446–2451.
24. Liu, C.; Yu, Z.; Neff, D.; Zhamu, A.; Jang, B. Z. Graphene-Based Supercapacitor with an Ultrahigh Energy Density. *Nano Lett.* **2010**, *10*, 4863–4868.
25. Stoller, M. D.; Park, S.; Zhu, Y.; An, J.; Ruoff, R. S. Graphene-Based Ultracapacitors. *Nano Lett.* **2008**, *8*, 3498–3502.
26. Lee, S. H.; Kim, H. W.; Hwang, J. O.; Lee, W. J.; Kwon, J.; Bielawski, C. W.; Ruoff, R. S.; Kim, S. O. Three-Dimensional Self-Assembly of Graphene Oxide Platelets into Mechanically Flexible Macroporous Carbon Films. *Angew. Chem., Int. Ed.* **2010**, *49*, 10084–10088.

27. Cao, X.; Shi, Y.; Shi, W.; Lu, G.; Huang, X.; Yan, Q.; Zhang, Q.; Zhang, H. Preparation of Novel 3D Graphene Networks for Supercapacitor Applications. *Small* **2011**, *7*, 3163–3168.

28. Du, F.; Yu, D. S.; Dai, L. M.; Ganguli, S.; Varshney, V.; Roy, A. K. Preparation of Tunable 3D Pillared Carbon Nanotube-Graphene Networks for High-Performance Capacitance. *Chem. Mater.* **2011**, *23*, 4810–4816.

29. Zhu, Y.; Murali, S.; Stoller, M. D.; Ganesh, K. J.; Cai, W.; Ferreira, P. J.; Pirkle, A.; Wallace, R. M.; Cychosz, K. A.; Thommes, M.; *et al.* Carbon-Based Supercapacitors Produced by Activation of Graphene. *Science* **2011**, *332*, 1537–1541.

30. Chen, Z.; Ren, W.; Gao, L.; Liu, B.; Pei, S.; Cheng, H.-M. Three-Dimensional Flexible and Conductive Interconnected Graphene Networks Grown by Chemical Vapour Deposition. *Nat. Mater.* **2011**, *10*, 424–428.

31. Agrawal, M.; Pich, A.; Gupta, S.; Zafeiropoulos, N. E.; Simon, P.; Stamm, M. Synthesis of Novel Tantalum Oxide Sub-micrometer Hollow Spheres with Tailored Shell Thickness. *Langmuir* **2008**, *24*, 1013–1018.

32. Ding, X.; Yu, K.; Jiang, Y.; Hari, B.; Zhang, H.; Wang, Z. A Novel Approach to the Synthesis of Hollow Silica Nanoparticles. *Mater. Lett.* **2004**, *58*, 3618–3621.

33. Huang, Z.; Tang, F. Preparation, Structure, and Magnetic Properties of Mesoporous Magnetite Hollow Spheres. *J. Colloid Interface Sci.* **2005**, *281*, 432–436.

34. Lee, J.-S.; Jung, C.-H.; Jo, S.-Y.; Choi, J.-H.; Hwang, I.-T.; Nho, Y.-C.; Lee, Y.-M.; Lee, J.-S. Preparation of Sulfonated Crosslinked Poly(2,6-dimethyl-1,4-phenylene oxide) Membranes for Direct Methanol Fuel Cells by Using Electron Beam Irradiation. *J. Polym. Sci., Part A: Polym. Chem.* **2010**, *48*, 2725–2731.

35. Lee, J.-S.; Ahn, H.-J.; Yoon, J.-C.; Jang, J.-H. Three-Dimensional Nano-Foam of Few-Layer Graphene Grown by CVD for DSSC. *Phys. Chem. Chem. Phys.* **2012**, *14*, 7938–7943.

36. Chen, J.; Minett, A. I.; Liu, Y.; Lynam, C.; Sherrell, P.; Wang, C.; Wallace, G. G. Direct Growth of Flexible Carbon Nanotube Electrodes. *Adv. Mater.* **2008**, *20*, 566–570.

37. He, Z.; Maurice, J.-L.; Gohier, A.; Lee, C. S.; Pribat, D.; Cojocaru, C. S. Iron Catalysts for the Growth of Carbon Nanofibers: Fe, Fe₃C or Both?. *Chem. Mater.* **2011**, *23*, 5379–5387.

38. Xu, S.; Zhang, J.; Zhong, M.; Liu, Y.; Zhang, Z.; Chen, H.; He, Z. Preparation and Magnetic Properties for Supersaturated Fe−C Solid Solution with Nanocrystalline Structure. *J. Magn. Magn. Mater.* **2005**, *292*, 126–134.

39. Dong, X. L.; Zhang, Z. D.; Xiao, Q. F.; Zhao, X. G.; Chuang, Y. C.; Jin, S. R.; Sun, W. M.; Li, Z. J.; Zheng, Z. X.; Yang, H. Characterization of Ultrafine γ-Fe(C), α-Fe(C) and Fe₃C Particles Synthesized by Arc-Discharge in Methane. *J. Mater. Sci.* **1998**, *33*, 1915–1919.

40. Grosvenor, A. P.; Kobe, B. A.; Biesinger, M. C.; McIntyre, N. S. Investigation of Multiplet Splitting of Fe 2p XPS Spectra and Bonding in Iron Compounds. *Surf. Interface Anal.* **2004**, *36*, 1564–1574.

41. Suzuki, S.; Yanagihara, K.; Hirokawa, K. XPS Study of Oxides Formed on The Surface of High-Purity Iron Exposed to Air. *Surf. Interface Anal.* **2000**, *30*, 372–376.

42. Bae, S.; Kim, H.; Lee, Y.; Xu, X.; Park, J.-S.; Zheng, Y.; Balakrishnan, J.; Lei, T.; Ri Kim, H.; Song, Y. I.; *et al.* Roll-to-Roll Production of 30-Inch Graphene Films for Transparent Electrodes. *Nat. Nanotechnol.* **2010**, *5*, 574–578.

43. Zhao, B.; Liu, P.; Jiang, Y.; Pan, D.; Tao, H.; Song, J.; Fang, T.; Xu, W. Supercapacitor Performances of Thermally Reduced Graphene Oxide. *J. Power Sources* **2012**, *198*, 423–427.

44. Lu, X.; Dou, H.; Gao, B.; Yuan, C.; Yang, S.; Hao, L.; Shen, L.; Zhang, X. A Flexible Graphene/Multiwalled Carbon Nanotube Film as a High Performance Plectrode Material for Supercapacitors. *Electrochim. Acta* **2011**, *56*, 5115–5121.

45. Marti, M.; Fabregat, G.; Estrany, F.; Aleman, C.; Armelin, E. Nanostructured Conducting Polymer for Dopamine Detection. *J. Mater. Chem.* **2010**, *20*, 10652–10660.

46. Wu, Z.-S.; Winter, A.; Chen, L.; Sun, Y.; Turchanin, A.; Feng, X.; Müllen, K. Three-Dimensional Nitrogen and Boron Co-doped Graphene for High-Performance All-Solid-State Supercapacitors. *Adv. Mater.* **2012**, *24*, 5130–5135.

47. Lai, L.; Yang, H.; Wang, L.; Teh, B. K.; Zhong, J.; Chou, H.; Chen, L.; Chen, W.; Shen, Z.; Ruoff, R. S.; *et al.* Preparation of Supercapacitor Electrodes through Selection of Graphene Surface Functionalities. *ACS Nano* **2012**, *6*, 5941–5951.